Sixth International Conference on
Enhanced, Compact and Ultra-Compact Heat Exchangers: Science, Engineering and Technology

CHE2007 – 0017

RESEARCH AND DEVELOPMENT OF HIGH-PERFORMANCE COMPACT FINLESS HEAT EXCHANGER

N. Shikazono[*1], D. Okawa[*1], M. Kobayashi[*1], N. Kasagi[*1], T. Waki[*2] , I. Kandori[*3] and S. Hataya[*4]

[*1] Department of Mechanical Engineering, The University of Tokyo, Tokyo, Japan; shika@feslab.t.u-tokyo.ac.jp
*2 Waki Factory, Inc., Saitama, Japan; w-tune@waki-ss.co.jp
*3 Kandori Weld Techno Industry, Aichi, Japan; weld-tec@kandori.jp
*4 Iwamoto, Co., Ltd., Tokyo, Japan; nrt@ar.wakwak.com

ABSTRACT

A concept of finless heat exchanger, which is composed of micro tubes without conventional fins, is proposed and assessed for achieving high performance and compactness. In reality, however, the precise assembly of numerous micro tubes leads to high manufacturing cost, and even small deviation of assembled tubes may cause considerable deterioration in heat exchanger performance. To resolve these issues, the micro tubes are connected and fixed in the streamwise direction, so that the manufacturability and quality of the micro finless heat exchanger could be drastically improved. In the present study, the basic characteristics of new tube arrangements, i.e., side-contacted and flat tubes, have been investigated through numerical simulation and experiment. As a result, it is found that the pressure loss of side-contacted tubes is always smaller than the detached tubes for given volume and heat exchange rate. Also, fully flat tubes show comparable performance to the side-contacted tubes. For side-contacted and fully flat tubes, empirical correlations of heat transfer coefficient and pressure drop are proposed. Finally, side-contacted and flat tube finless heat exchangers are fabricated and evaluated through experiment. The measured heat exchange rate and pressure drop show satisfactory agreement with the proposed correlations.

INTRODUCTION

Great efforts have been made for heat transfer augmentation, and a number of compact heat exchanger designs have been proposed to date (e.g., Kays and London, 1984). Most of the compact gas-liquid heat exchangers utilize fins in order to compensate a lower heat transfer rate on the gas side. Paitoonsurikarn et al. (2000) proposed a micro bare-tube heat exchanger, which was composed of a bundle of small diameter tubes without conventional fins. Kasagi et al. (2003) optimized micro bare-tube heat exchangers with a simulated annealing (SA) method using the trained neural network representing the heat transfer and pressure drop characteristics of a specified tube bank. It was shown that the micro bare-tube heat exchanger had a possibility of improving heat transfer performance and compactness with its high over-all heat transfer rate and large heat transfer area density.

Although micro bare-tube heat exchanger shows excellent heat transfer performance, difficulties in handling and sealing numerous small tubes are the hurdles for mass production. Furthermore, robustness against tube pitch variation is required because even a small deviation may deteriorate heat exchanger performance. If the tubes were connected and fixed in the streamwise direction, in other words, if connected tubes or flat tubes can be used, accurate positioning of the tubes and reliable sealing can be achieved. Besides, extrusion molding or press molding can be used for their fabrication. These are favorable features for cost reduction and quality control.

One of the major difficulties in designing compact heat exchangers is the accurate estimation of heat transfer rate and pressure drop to assess the trade-off between compactness, heat exchange capacity, pumping power and fan noise. Thus, it is important to estimate accurately both heat transfer rate and pressure drop of the air-side flow. Paitoonsurikarn et al. (2000) utilized the heat transfer and pressure drop correlations proposed by Zukauskas (1972). However, those correlations are not verified for predicting a wide range of tube arrangements and also at low Reynolds numbers, e.g., $Re < 500$, which is a characteristic Re range for compact heat exchangers. One of the main objectives of this study is to propose a reliable optimization method for designing fin less heat exchangers.

In the present study, the basic characteristics of new tube arrangements, i.e., side-contacted and flat tubes, have

been investigated through numerical simulation. For side-contacted and flat tubes, empirical correlations of heat transfer coefficient and pressure drop are proposed. Finally, side-contacted and flat tube finless heat exchangers are fabricated and evaluated through experiment.

NUMERICAL SIMULATION

Numerical Method

A commercial CFD code, FLUENT6.0, is employed to calculate the flow and thermal fields around tube bundles with 3 rows in the transverse direction and 10 columns in the longitudinal direction as shown in Fig. 1. The tube surface is assumed to be isothermal. Periodic boundary condition is employed in the transverse direction, and uniform velocity and free outflow conditions are given at inlet and outlet boundaries, respectively. The temperature dependence of the physical properties of working fluids is neglected. Oku et al. (2003) reported that the predicted Strouhal numbers and drag coefficients from simulations of 120 and 360 tube surface grid points are negligible. Thus, 120 grid points were used for each tube surface.

The Reynolds number based on the tube diameter and the frontal velocity, Re_f, is varied in the range of Re_f=10 to 200. According to Kasagi et al. (2003), the optimal dimensionless transverse and longitudinal tube pitches are around $P_T = 2.3 \sim 2.5$, $P_L \fallingdotseq 1.3$ for any optimization conditions. In the present study, numerical simulation is performed for the tube pitch conditions in the range of $P_T = 2 \sim 4$, $P_L = 1 \sim 2.5$ in order to focus on the narrow range

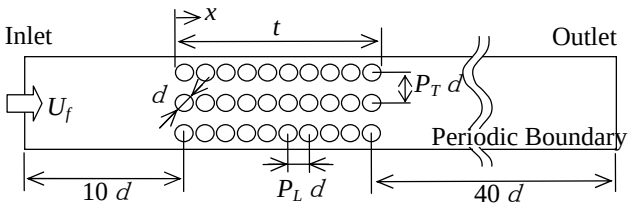

Fig. 1 Computational domain

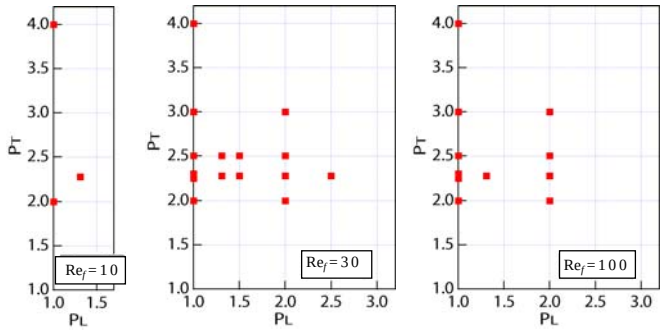

Fig. 2 Tube pitch conditions

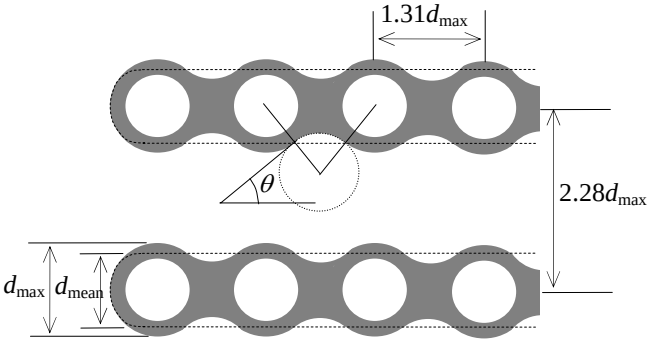

Fig. 3 Cross section of wavy extruded tube

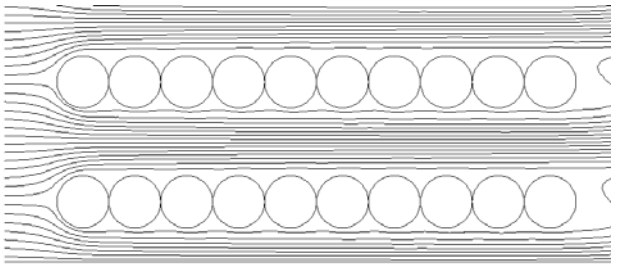

(a) Side-contacted tube bank (P_T =2.5, P_L=1.0)

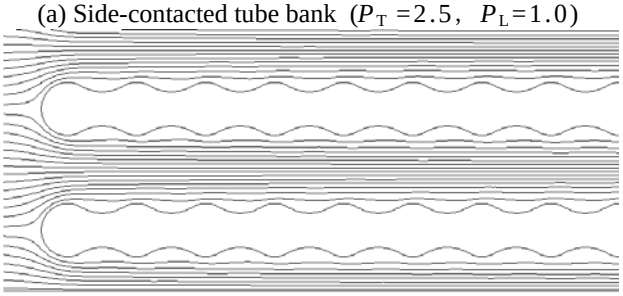

(b) Wavy flat tube

Fig. 4 Typical stream lines at Re_f =100

around the optimal point as shown in Fig. 2. For flat tubes, tubes with P_T =2.28 and P_L =1.31 are connected with a tangential arc as shown in Fig. 3. The tube becomes fully flat when contact angle becomes $\theta = 0^\circ$. Figure 4 shows the stream lines between the rows at Re_f =100. The flows between the rows are stable and nearly parallel except for the region vicinity to the tube surface.

Effects of Longitudinal Tube Pitch P_L

Heat transfer and pressure drop of tube bundles with different longitudinal pitches P_L are evaluated. Figure 5 shows the predicted pressure losses for various P_L tubes. Comparison is made with a side-contacted tube bundle (P_L=1.0) of same heat exchange rate, frontal area, volume, tube diameter and flow rate. The number of tubes and transverse pitch of the side-contacted case were varied so that they give same volume and heat exchange rate for each comparison. Thus, the pressure losses of side-contacted and

detached tubes with same volume and capacity can be directly compared. The pressure losses of side-contacted

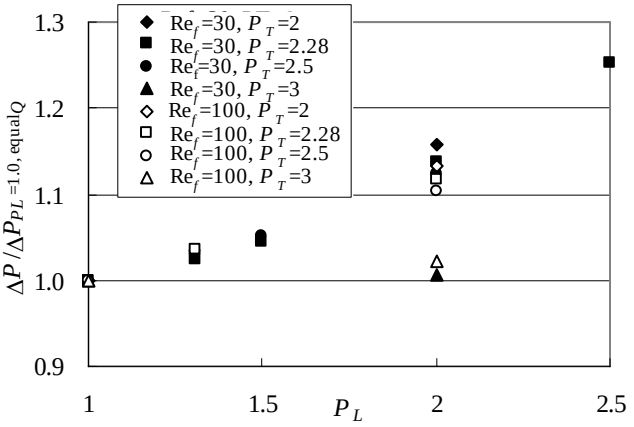

Fig. 5 Pressure loss for given volume and heat exchange rate (Comparison with P_L=1 side-contacted tubes)

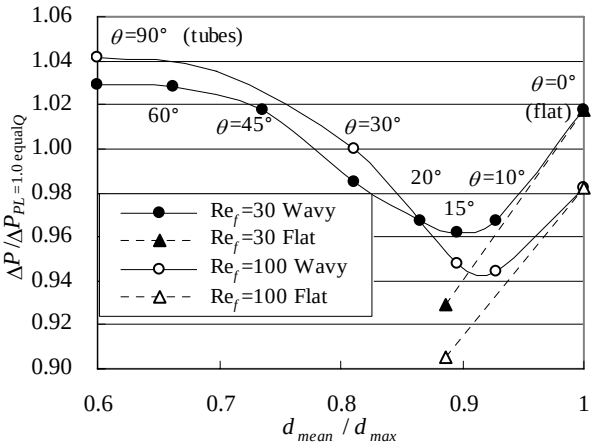

Fig. 6 Pressure loss for given volume and heat exchange rate (Wavy extruded tube)

tubes were always smaller than detached tubes as shown in Fig. 5. This is because transverse tube pitches of side-contacted tubes can be increased for given KA value and volume.

The flow inside the gap between the tubes is stagnated and the temperature difference is very small. Thus, the gap region has negligible contribution to the total heat exchange. Oku et al. (2003), Kasagi et al. (2003) investigated heat transfer and pressure drop characteristics of tube bundles with wide range of dimensionless pitch (P_T, P_L=1.25～4.5), and reported that the optimal longitudinal pitch was around $P_L \fallingdotseq 1.3$. It is clearly shown from the present study focusing on the narrow range around the optimal point that the side-contacted tubes are superior than the detached tubes. In addition, side-contacted tubes provide largest in-tube heat transfer area, so the total heat resistance can be further reduced compared to detached cases.

Flat Tubes with Wavy Surface

Figure 6 shows the effects of the flat tube wave pattern. The abscissa represents the mean thickness d_{mean} which corresponds to the contact angle θ of the arc connecting the P_T =2.28 and P_L =1.31 tubes (see Fig. 1). Pressure loss comparison was made between the side-contacted tubes (diameter = d_{max}, P_L=1) of same volume and heat exchange rate. The pressure loss curves for both Re_f=30 and 100 take minimum values around θ =10～15 degrees. The dashed lines in Fig. 6 are the results for fully flat tubes without roughness but of same thickness d_{mean}. For small wave amplitudes, wavy tube and fully flat tube with same mean tube thickness are nearly identical. This implies that air can flow along the wavy surface when surface roughness is small, but separation at the wave crest occurs and the pressure drop increases for larger roughness.

It is also shown that the pressure loss of fully flat tube without roughness (θ =0°, d_{mean}/d_{max}=1) is nearly identical to the side-contacted tube bundles. The difference is within ±2%, which means that the heat exchange performances of fully flat tubes without roughness (θ =0) and side-contacted tube bundles are nearly identical in a practical sense.

PREDICTIVE EQUATIONS FOR SIDE-CONTACTED (P_L=1) AND FULLY FLAT TUBES

Predictive equations for side-contacted tube bundles are developed using the CFD data. The model is composed of two regions, i.e., first tube region ($0<x \leqq d$) and the channel region after the second column ($d<x \leqq t$).

Nusselt number and the drag coefficient for the first tube region ($0<x \leqq d$) are obtained by the least square fitting of the numerical simulation data as follows:

$$Nu_1 \equiv \frac{h_1 d}{\lambda} = 0.85\left(\frac{P_T}{P_T - 1}\right)^{0.6} \mathrm{Pr}^{0.33}\,\mathrm{Re}_f^{0.38}, \qquad (1)$$

$$C_{D1} \equiv \frac{\Delta P_1}{\rho U_f^2/2} P_T = 2.95\left(\frac{P_T}{P_T - 1}\right)^{2.7} \mathrm{Re}_f^{-0.32}, \qquad (2)$$

where U_f is the frontal air velocity and Re_f is the Reynolds number defined by U_f and tube diameter d.

For the channel region after the second column ($d<x \leqq t$), effective channel height H and hydraulic diameter D are introduced for both velocity and temperature fields to express the wavy roughness effects as follows:

$$D_{temp} = 2H_{temp} = 2(P_T - 0.855)d, \qquad (3)$$

$$D_{vel} = 2H_{vel} = 2(P_T - 0.930)d. \qquad (4)$$

In order to express the entrance developing effect, empirical equation of Stephan (1959) is utilized.

$$Nu_{\text{entry}} \equiv \frac{h_{\text{entry}} D_{\text{temp}}}{\lambda} = \frac{2}{\pi}\left[7.55 + \frac{0.024\left(x^*_{\text{temp}}\right)^{-1.14}}{1+0.0358\left(x^*_{\text{temp}}\right)^{-0.64}\,\text{Pr}^{0.17}}\right]. \quad (5)$$

The coefficient $2/\pi$ in the R.H.S appears because heat transfer area is defined by the tube surface. Same functional form is adopted for the friction factor, and the coefficients are chosen by the least square fitting of the CFD results.

$$f_{\text{entry}} \equiv \frac{\Delta P_{\text{entry}}}{\rho U_{\text{ch}}^2/2}\frac{D_{\text{vel}}}{4x} = \frac{1}{\text{Re}_{\text{ch}}}\left[24 + \frac{0.1\left(x^*_{\text{vel}}\right)^{-1.05}}{1+0.01\left(x^*_{\text{vel}}\right)^{-0.8}}\right], \quad (6)$$

where,

$$x^*_{\text{temp}} = \frac{x}{D_{\text{temp}}\,\text{Re}_{\text{ch}}\,\text{Pr}}, \quad (7)$$

$$x^*_{\text{vel}} = \frac{x}{D_{\text{vel}}\,\text{Re}_{\text{ch}}}, \quad (8)$$

$$\text{Re}_{\text{ch}} = \frac{D_{\text{vel}} U_{\text{ch}}}{\nu}, \quad (9)$$

$$U_{\text{ch}} = \frac{P_{\text{T}} d}{H_{\text{vel}}} U_{\text{f}}. \quad (10)$$

Eliminating the effects of first tube region ($0 < x \leqq d$), Nusselt number and friction factor for the channel region ($d < x \leqq t$) are obtained as follows:

$$Nu_{\text{ch}} \equiv \frac{h_{\text{ch}} D_{\text{temp}}}{\lambda} = \frac{t \cdot Nu_{\text{entry}}\big|_{x=t} - d \cdot Nu_{\text{entry}}\big|_{x=d}}{t-d}, \quad (11)$$

$$f_{\text{ch}} \equiv \frac{\Delta P_{\text{ch}}}{\frac{\rho U_{\text{ch}}^2}{2}}\frac{D_{\text{vel}}}{4(t-d)} = \frac{t \cdot f_{\text{entry}}\big|_{x=t} - d \cdot f_{\text{entry}}\big|_{x=d}}{t-d}. \quad (12)$$

Finally, average heat transfer coefficient and pressure drop can be obtained using Eqs. (1), (2), (11) and (12)as follows:

$$h_{\text{mean}} = \frac{\frac{Nu_1 \lambda}{d} d + \frac{Nu_{\text{ch}} \lambda}{D_{\text{temp}}}(t-d)}{t}, \quad (13)$$

$$\Delta P = \Delta P_1 + \Delta P_{\text{ch}} = C_{\text{D1}} \frac{\rho U_{\text{f}}^2}{2}\frac{1}{P_{\text{T}}} + f_{\text{ch}} \frac{\rho U_{\text{ch}}^2}{2}\frac{4(t-d)}{D_{\text{vel}}}. \quad (14)$$

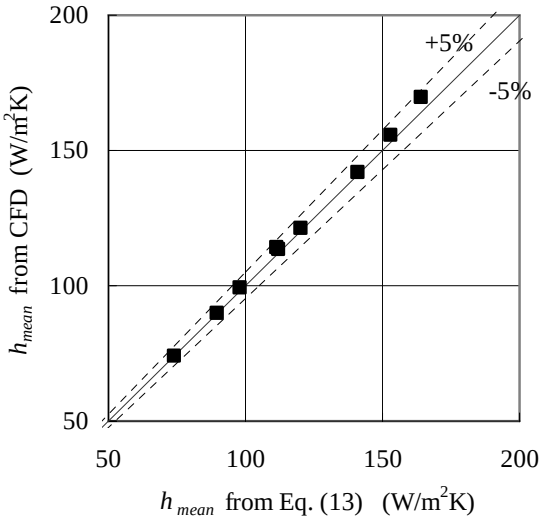

Fig. 7 Comparison of mean heat transfer coefficient from Eq. (13) and CFD data

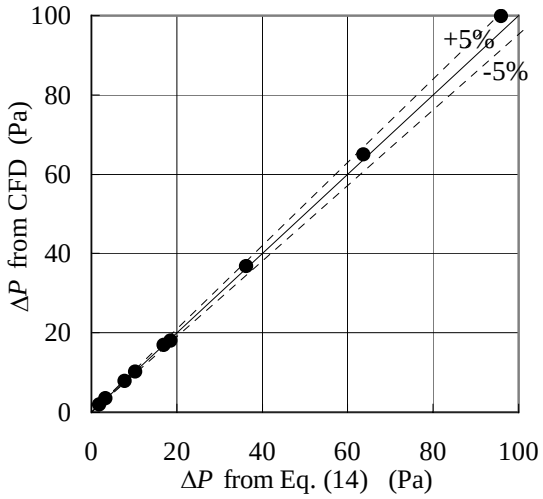

Fig. 8 Comparison of pressure drop from Eq. (14) and CFD data

Figures 7 and 8 show the comparison between CFD data and the predictions from Eqs. (13) and (14). The parameter range is Re_{f} =30～200, P_{T} =2～3, P_{L} =1. Heat transfer coefficient and pressure drop can be predicted within ±5% error against CFD results.

As already discussed in the previous section, the difference between side-contacted tubes and fully flat tubes without wavy roughness is small in a practical sense. Thus, Eqs. (1) to (14) can be used for the fully flat tubes. For this case, hydraulic diameters in Eqs. (3) and (4) should be modified as $D_{\text{temp}} = D_{\text{vel}} = 2(P_{\text{T}} - 1.0)d$, and the coefficient $2/\pi$ in Eq. (5) should be replaced by 1.

EXPERIMENTAL VALIDATION

Side-contacted Tubes

A heat exchanger composed of side-contacted tubes is fabricated. Specification of the tested heat exchanger is listed in Table 1. The copper tubes of ϕ0.3mm diameter are connected in the longitudinal direction (P_L=1), with transverse pitch of P_T =2.5. Figure 9 shows the experimental setup. Hot water is provided by the pump to the test sample. Heat exchange rate was measured by both air side and water side and the difference was less than 5%. Air outlet temperature and velocity were measured by 28 points at 15mm downstream of the heat exchanger. Inlet air and water temperatures were 27℃ and 52℃, respectively.

Figure 10 shows the measured and predicted air side pressure drop. Experimental data is 8% larger than the prediction by Eq. (14). Velocity distribution downstream of the heat exchanger measured by pitot tube shows large variation as is shown in Fig. 11. According to Eq. (14), 10μm difference in transverse tube pitch results in 4% pressure drop difference. The tubes of the test sample show slight deflection at the center, and the low velocity region seems to correspond to the deflected area. Thus, it is considered that slight tube pitch variation which is caused during the fabricating process affected the velocity distribution and the pressure drop.

Figure 12 shows the measured and predicted heat exchange rates using Eq. (15) and the ε-*NTU* method. Prediction shows good agreement with the experimental data for the heat exchange rate.

Fully Flat Tubes

Figure 13 shows the fabricated fully flat tube heat exchanger. Specification is listed on Table 2. Since heat resistance at the tube wall is negligible, present fully flat tube heat exchanger was made of stainless steel and was fabricated by press work and brazing. The experiment is performed using the same setup described in the previous section. Inlet air and water temperatures were set as 20℃ and 57℃, respectively. The water flow rate was G_w=200 g/min for this case.

Table 1 Specifications of the side contacted tube heat exchanger

Tube Outer Diameter d mm	Tube Inner Diameter d_i mm	Tube length l mm	Streamwise Thickness t mm	Spanwise Width w mm
0.3	0.24	86	6.6 (P_L = 1.0)	21.75 (P_T = 2.5)

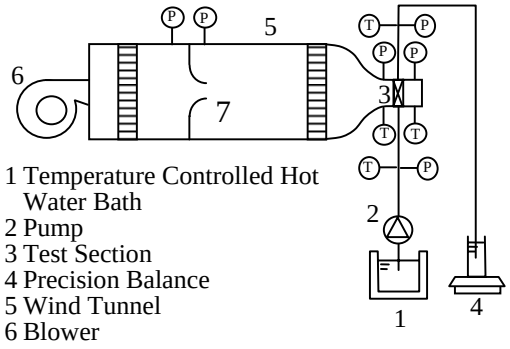

Fig. 9 Experimental Setup

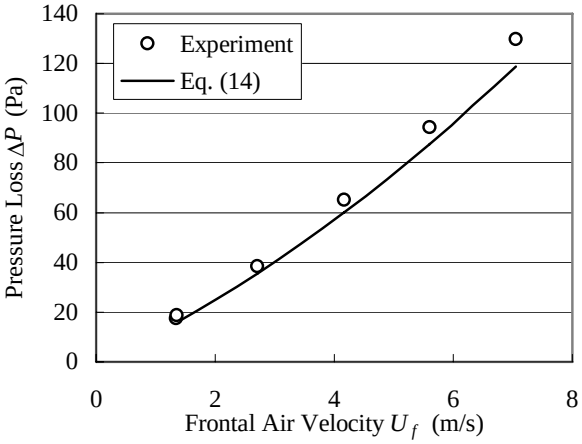

Fig. 10 Predicted and Measured Pressure Loss

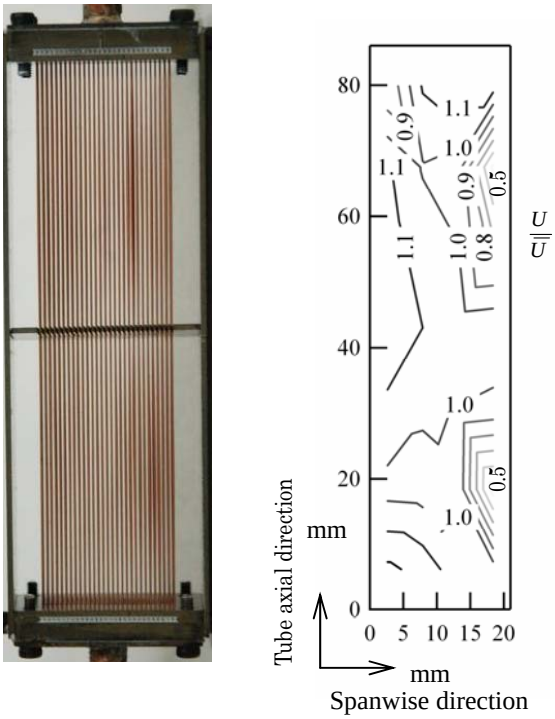

Fig. 11 Contour map of normalized velocity distribution

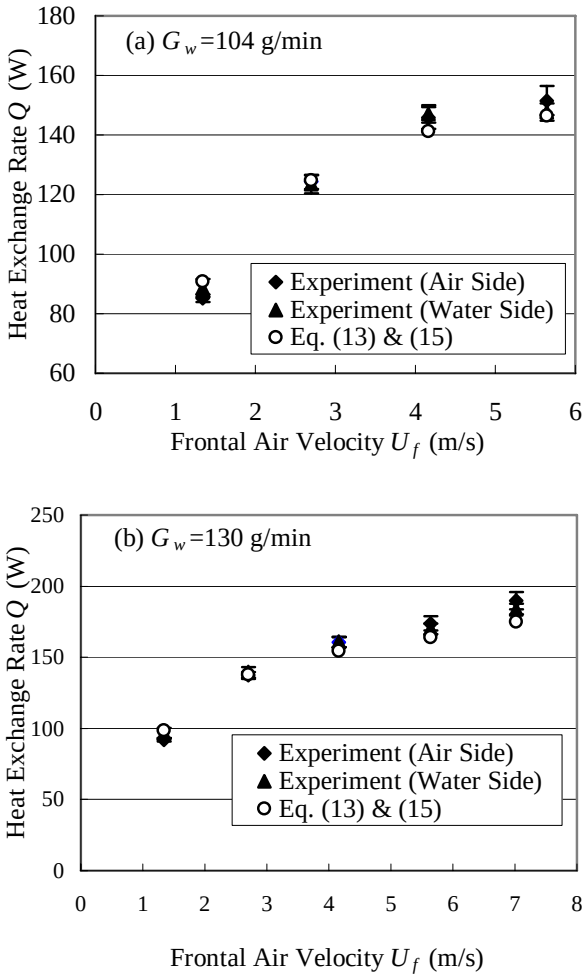

Fig.12 Measured and predicted heat exchange rate.
(a) G_w=104 g/min, (b) G_w=130 g/min

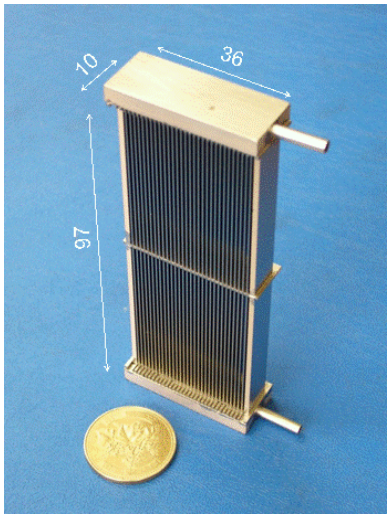

Fig.13 Fully flat SUS tube finless heat exchanger

Table 2 Specifications of the fully flat tube heat exchanger

Tube Outer Thickness d mm	Tube pitch mm	Tube length l mm	Streamwise Thickness t mm	Spanwise Width w mm
0.54	1.2	97	10	36

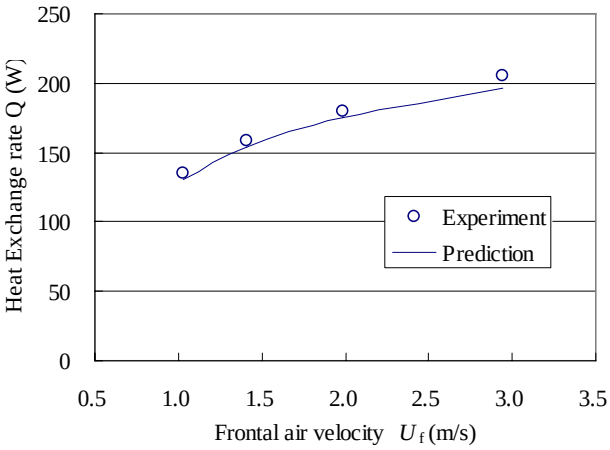

Fig.14 Measured and predicted heat exchange rate

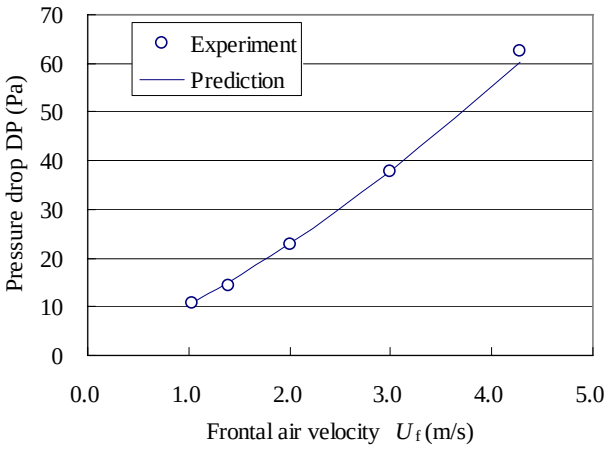

Fig.15 Measured and predicted pressure drop

Figures 14 and 15 show the measured heat transfer rate and air side pressure drop. Predictions by Eqs. (14) and (15) are also shown in the figures. Good agreement is achieved for both heat transfer rate and pressure drop. More than 150 W is obtained with inlet temperature difference of ΔT=37℃.

CONCLUSIONS

Side-contacted tube and flat tube finless heat exchangers are evaluated by numerical simulation and

experiment. In the present study, the following conclusions are derived:

1. Side-contacted tube arrangement ($P_L=1$) gives smaller pressure drop than detached tube arrangement for given volume and heat exchange rate.
2. Pressure drop of wavy flat tubes becomes minimum when the contact angle of the arc is around $\theta=10\sim$ 15 degrees. The heat exchange performances of fully flat tubes without roughness ($\theta=0$, $d_{mean}/d_{max}=1$) and side-contacted tube bundles are practically identical.
3. Predictive equations of heat transfer coefficient and pressure drop for side-contacted and fully flat tube heat exchangers are developed. Proposed correlations can predict heat transfer coefficient and pressure drop within $\pm$5% error against the CFD results.
4. Fabricated side-contacted tube heat exchanger showed larger pressure drop due to the slight tube pitch variation. Measured heat exchange rate showed good agreement with the prediction.
5. The experimental data for the fully flat tube heat exchanger made of stainless steel showed good agreement with the prediction. More than 150 W can be obtained with inlet temperature difference of ΔT=37℃.

ACKNOWLEDGEMENT

The authors would like to thank Prof. Y. Suzuki at the University of Tokyo for the beneficial discussion.

NOMENCLATURE

A	Heat transfer area, [m^2]
C_D	Drag coefficient, [-]
d	Tube diameter, [m]
D	Hydraulic diameter, [m]
f	Friction factor, [-]
G	Mass flow rate, [g/min]
h	Heat transfer coefficient, [W/m^{2}K]
H	Effective channel height, [m]
l	Heat exchanger length, [m]
Nu	Nusselt number, [-]
p	Pressure, [Pa]
P_T	Dimensionless transverse pitch, [-]
P_L	Dimensionless longitudinal pitch, [-]
Pr	Prandtl number, [-]
Q	Heat exchange rate, W
Re	Reynolds number, [-]
t	Heat exchanger thickness, [m]
T	Temperature, [K]
U	Velocity, [m/s]
w	Heat exchanger width, [m]
P	Pressure, [Pa]
x	Streamwise location, [m]
λ	Thermal conductivity, W/mK
θ	Contact angle of the arc, [deg]
ρ	Density, [kg/m^3]

Subscript

a	Air side
ch	Channel region
entry	Entry region
f	Frontal
max	Max
mean	Mean
temp	Temperature field
vel	Velocity field
w	Water side
1	First tube region

REFERENCES

Oku, T., Kasagi, N. and Suzuki, Y., 2003, Optimum Design of Micro Bare-Tube Heat Exchanger (in Japanese), *Transactions of the JSME*, Series B, 69-686, 2313-2320.

Kasagi, N., Suzuki, Y., Shikazono, N. and Oku, T., 2003, Optimal Design and Assessment of High Performance Micro Bare-Tube Heat Exchangers, *Proc. 4th Int. Conf. on Compact Heat Exchangers and Enhancement Technologies for the Process Industries*, pp. 241-246.

Paitoonsrikarn, S., Kasagi N. and Suzuki, Y., 2000, Optimal Design of Micro Bare-Tube Heat Exchanger, Proc. Symp. Energy Eng. in the 21st Century, Vol. 3, pp. 972-979.

Stephan, K., 1959, Warmeubergang und druckabfall bei nicht ausgebildeter Laminarstromung in Rohren und in in ebenen Spalten, *Chem.-Ing.-Tech.*, 31, pp. 773-778.

Zukauskas, A., 1972, Heat Transfer from Tubes in Cross Flow, *Adv. in Heat Transfer*, pp. 93-160.